

**Rational valence modulation of bimetallic carbide assisted by defect engineering
to enhance polysulfide conversion for lithium-sulfur batteries**

Ting Yang ^{a,b}, Kunlin Liu ^{a,b}, Tianli Wu ^{a,b}, Jizong Zhang ^{a,b}, Xuewen Zheng ^{a,b},
Chengyang Wang ^{a,b}, Mingming Chen ^{a,b,*}.

^a Key Laboratory for Green Chemical Technology of MOE, School of Chemical Engineering and Technology, Tianjin University, Tianjin 300072, P. R. China

^b Collaborative Innovation Center of Chemical Science and Engineering (Tianjin), Tianjin 300072, P. R. China

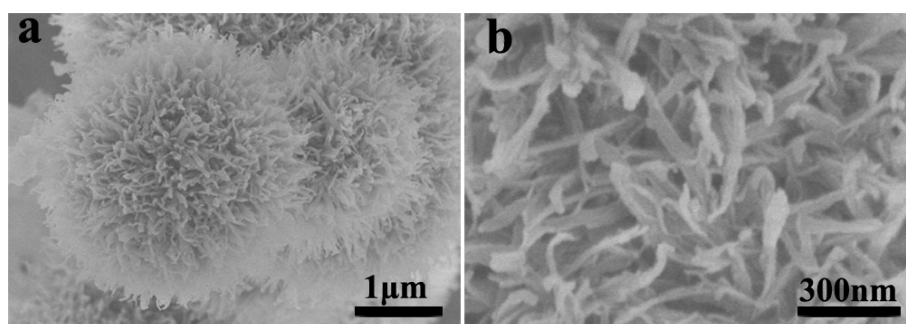


Figure S1. The SEM (a) and HRSEM (b) images of NiZn-MOF.

As shown in Figure S1 a, NiZn-MOF composites exhibit a flower-like structure with a diameter of about 3.5 ~ 2.5 μm. The HRSEM image (Figure S2 b) indicates that NiZn-MOF composites are consisted of abundant nanosheets, which is beneficial to expose more active sites.

* Corresponding author:

Tel: +86-22-27890481. E-mail: chmm@tju.edu.cn (Mingming Chen)

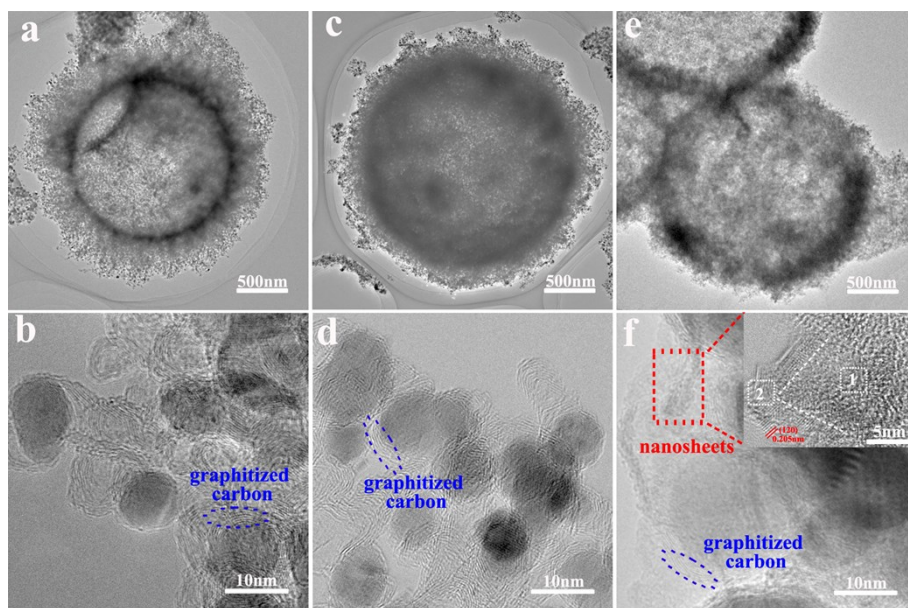


Figure S2. (a-b) The TEM images of $C/Ni_3ZnC_{0.7}$ nanospheres. (c-d) The TEM images of $C/Ni_3ZnC_{0.7}$ -P5 nanospheres. (e-f) The TEM images of $C/Ni_3ZnC_{0.7}$ -B1 nanospheres. The inset is the corresponding HRTEM image of figure f.

As shown in Figure S2, $C/Ni_3ZnC_{0.7}$, $C/Ni_3ZnC_{0.7}$ -P5 and $C/Ni_3ZnC_{0.7}$ -B1 nanospheres are composed of 8-15 nm nanoparticles with typical hollow structures. Such ultrathin nanoparticles and hollow structure contribute to dense exposure of active sites. The graphitized carbon shells might come from the catalytic graphitization behavior of $C/Ni_3ZnC_{0.7}$ nanoparticles, which is positive for charge transfer process.

Besides, after the $NaBH_4$ etching process, a bit of nanosheets are appearing on the surface of $C/Ni_3ZnC_{0.7}$ -B1. And the area with nanosheets is specifically chosen as shown in Figure S2 f. The close look of the nanosheet (Figure S2 f) indicates that it can be divided into two parts (donated as area 1 and 2). The amorphous area (area 1) should be attributed to amorphous nickel borides (Ni_xB), which comes from the reaction between the $Ni_3ZnC_{0.7}$ and $NaBH_4$. However, it should be noted that the crystalline structure of some nanoparticles in area 2 became robust under electron irradiation. And the short-range lattice fringe of 0.205 nm is corresponding to the (120)

planes of $\text{Ni}_3(\text{BO}_3)_2$ ¹. The formation of $\text{Ni}_3(\text{BO}_3)_2$ is attributed to the hydrolysis of NaBH_4 . The NaBH_4 itself could hydrolyze to obtain H_3BO_3 and such hydrolysis process could be accelerated by metal borides.^{1,2} Therefore, once the amorphous Ni_xB forms, the generation of borate anions (BO_3^{2-}) would be enhanced to accumulate around the nearly formed Ni_xB , followed by turning the amorphous Ni_xB to $\text{Ni}_3(\text{BO}_3)_2$ ^{1,2}.

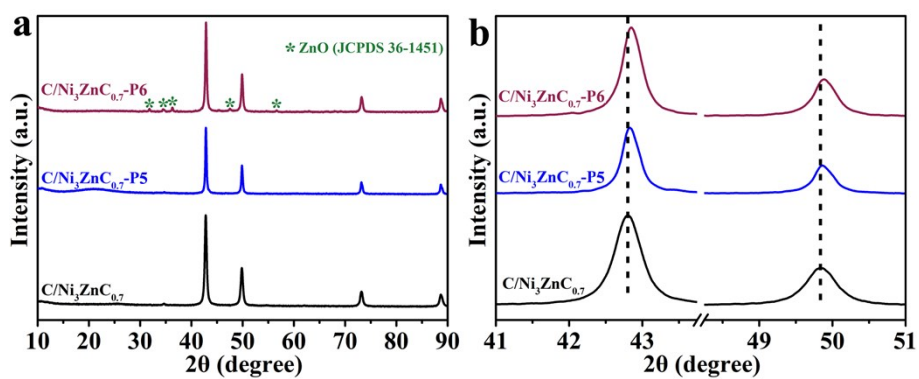


Figure S3. (a-b) The XRD patterns of $C/Ni_3ZnC_{0.7}$ nanospheres, $C/Ni_3ZnC_{0.7}$ -P5 nanospheres and $C/Ni_3ZnC_{0.7}$ -P6 nanospheres.

Although P atom is larger than C in atomic radius, the loss of Zn results in decreased lattice parameters,³ attested by the slightly positive shift of XRD peaks in $C/Ni_3ZnC_{0.7}$ -P5 and $C/Ni_3ZnC_{0.7}$ -P6 (Figure S3 b).

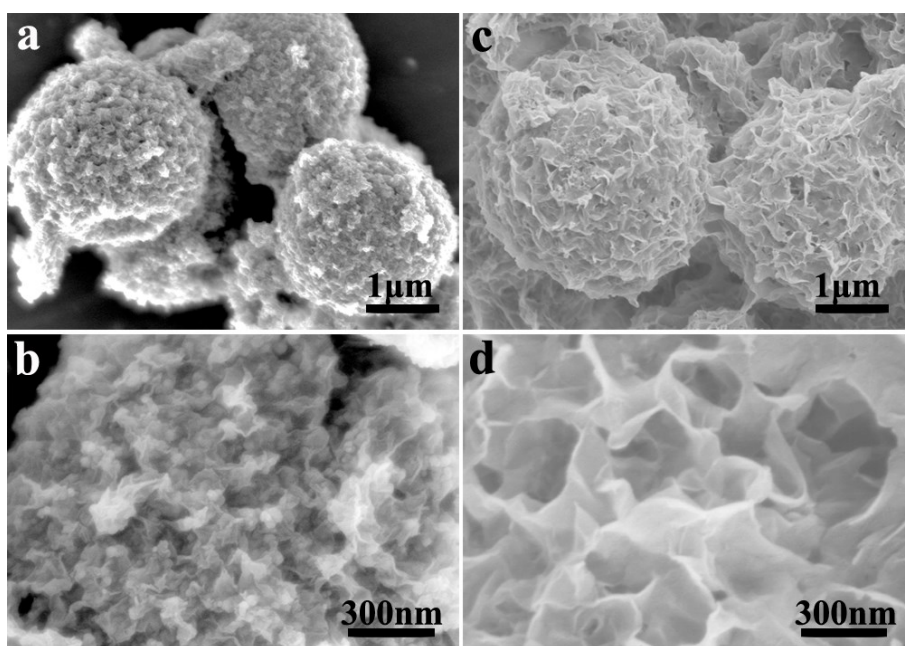


Figure S4 (a-b) The SEM images of C/Ni₃ZnC_{0.7}-B2 nanospheres. (c-d) The SEM images of C/Ni₃ZnC_{0.7}-B4 nanospheres.

As shown in Figure S4 a and b, when increasing the concentration of the NaBH₄ solution to 0.02 mol L⁻¹, more nanosheets appear on the surface of the C/Ni₃ZnC_{0.7}-B2 nanospheres, rendering slightly collapse of spherical structure. Further increasing the concentration of the NaBH₄ solution to 0.04 mol L⁻¹ (Figure S4 c and d), C/Ni₃ZnC_{0.7}-B4 are almost covered by plenty of nanosheets.

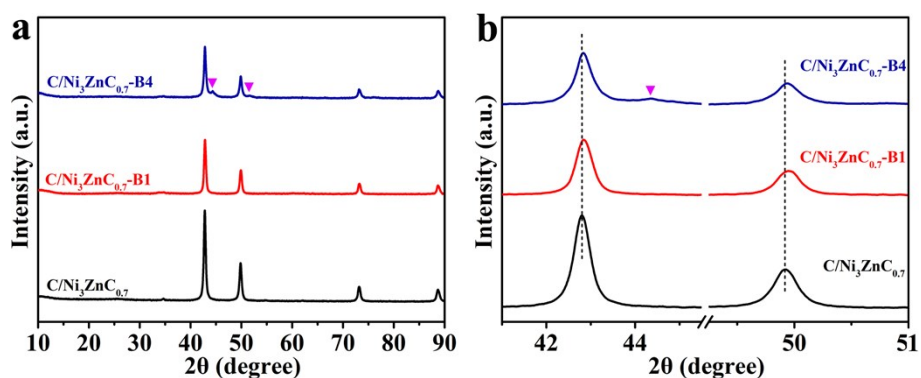


Figure S5. (a-b) The XRD patterns of C/Ni₃ZnC_{0.7} nanospheres, C/Ni₃ZnC_{0.7}-B1 nanospheres and C/Ni₃ZnC_{0.7}-B4 nanospheres.

When the concentration of NaBH₄ solution is 0.04 mol L⁻¹, C/Ni₃ZnC_{0.7}-B4 is covered by plenty of smooth nanosheets and presents a broad XRD peak at 44.4°, supporting the existence the amorphous Ni_xB phase (Figure S4 c-d and S5 a-b)^{1,4}. As the concentration of NaBH₄ solution decreases to 0.01 mol L⁻¹, the nanosheets become tiny as well as less and out of XRD detection range (Figure 1e-f, and S5 a-b). The amorphous Ni_xB phase indicates NaBH₄-etching process makes some Ni cations out of Ni₃ZnC_{0.7} lattice, rendering a Ni vacancy-rich structure. Besides, the loss of Ni leads to a slightly decreased lattice parameter,³ attested by the slightly positive shift of XRD peaks in C/Ni₃ZnC_{0.7}-B1 and C/Ni₃ZnC_{0.7}-B4 (Figure S5 b).

Table S1. The elemental content measured by EDS.

Samples	C (at/%)	O (at/%)	Zn (at/%)	Ni (at/%)	P (at/%)	B (at/%)
C/Ni₃ZnC_{0.7}	74.07	2.56	5.81	17.56	-	-
C/Ni₃ZnC_{0.7}-P5	26.33	10.99	14.51	46.78	1.38	-
C/Ni₃ZnC_{0.7}-B1	48.84	16.64	4.85	13.91	-	15.75

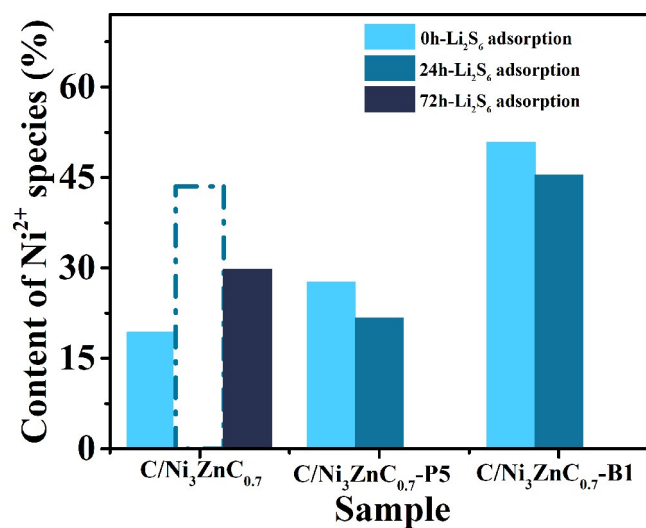


Figure S6. The content of Ni²⁺ species in different samples obtained by XPS.

Table S2. The content of Ni²⁺ and Ni(0) species in different samples obtained by XPS.

Samples	Ni²⁺ ration in Ni 2p region (%)	Ni(0) ration in Ni 2p region (%)	The ratio of Ni²⁺ to Ni(0)
Ni₃ZnC_{0.7}	19.12	66.69	0.29
Ni₃ZnC_{0.7}-P5	27.68	56.62	0.49
Ni₃ZnC_{0.7}-B1	50.83	15.76	3.23
Ni₃ZnC_{0.7}-Li₂S₆-24h	43.52	30.44	1.43
Ni₃ZnC_{0.7}-Li₂S₆-72h	29.75	51.89	0.57
Ni₃ZnC_{0.7}-P5-Li₂S₆-24h	21.65	62.80	0.34
Ni₃ZnC_{0.7}-B1-Li₂S₆-24h	45.40	29.13	1.56

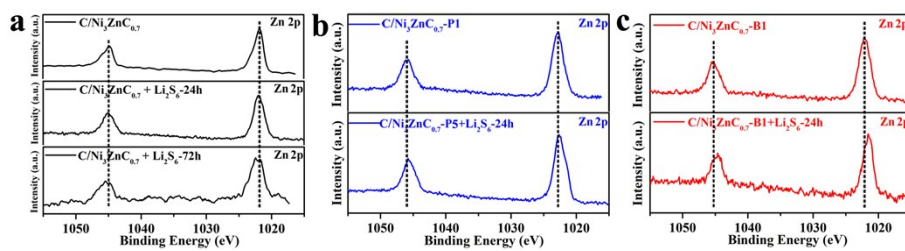


Figure S7. (a) High-resolution Zn 2p XPS spectra of C/Ni₃ZnC_{0.7} nanospheres before Li₂S₆ adsorption test, after adding in Li₂S₆ solution for 24 h and 72 h. (b) High-resolution Zn 2p XPS spectra of C/Ni₃ZnC_{0.7}-P5 nanospheres before and after adding in Li₂S₆ solution for 24 h. (c) High-resolution Zn 2p XPS spectra of C/Ni₃ZnC_{0.7}-B1 nanospheres before and after adding in Li₂S₆ solution for 24 h.

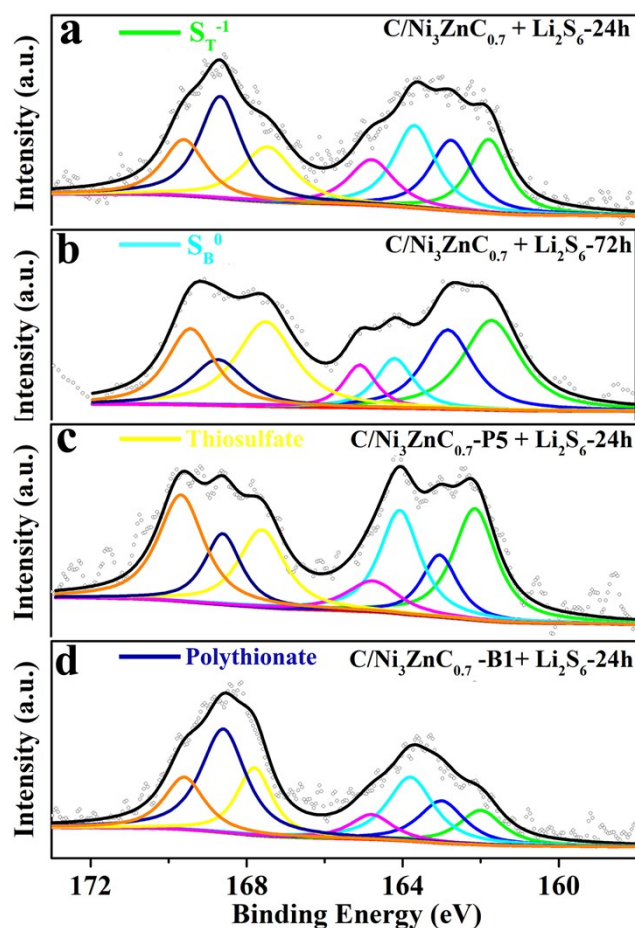


Figure S8. (a) High-resolution S 2p XPS spectra of C/Ni₃ZnC_{0.7} nanospheres after adding in Li₂S₆ solution for 24 h. (b) High-resolution S 2p XPS spectra of C/Ni₃ZnC_{0.7} nanospheres after adding in Li₂S₆ solution for 72 h. (c) High-resolution S 2p XPS spectra of C/Ni₃ZnC_{0.7}-P5 nanospheres after adding in Li₂S₆ solution for 24 h. (d) High-resolution S 2p XPS spectra of C/Ni₃ZnC_{0.7}-B1 nanospheres after adding in Li₂S₆ solution for 24 h.

Owing to the chemical interaction between polysulfides and metal active sites, thiosulfate and polythionate species located at 167.5 eV and 168.6 eV are generated at the surface of these three samples (Figure S8 a-d).⁵ The generation of thiosulfate comes from the oxidation of S₄²⁻ by Ni²⁺, thereby contributing to the decrease of Ni²⁺ species and increase of Ni(0) species (Figure S6 and Table S1).⁵ Such thiosulfate could anchor long-chain polysulfides to yield polythionate and Li₂S₂/Li₂S, which provides a new path for accelerating the conversion of polysulfides.⁶

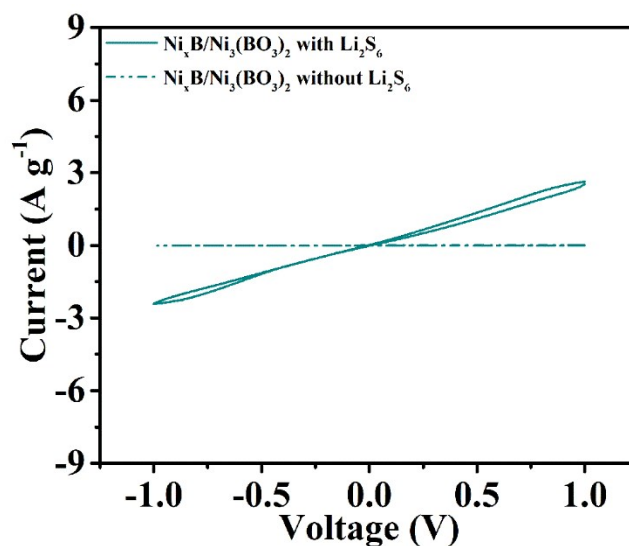


Figure S9. CV curves of symmetric cell with identical electrodes of $\text{Ni}_x\text{B}/\text{Ni}_3(\text{BO}_3)_2$ using Li_2S_6 electrolyte or Li_2S_6 -free electrolyte at a scan rate of 10 mV s^{-1} .

The $\text{Ni}_x\text{B}/\text{Ni}_3(\text{BO}_3)_2$ nanosheets were synthesized by adding the NaBH_4 into the $\text{Ni}(\text{NO}_3)_2$ solution according to the previously reported work.⁷ And the symmetric cells were assembled by using $\text{Ni}_x\text{B}/\text{Ni}_3(\text{BO}_3)_2$ electrodes as working and counter electrodes, $40 \mu\text{L}$ Li_2S_6 solution (1.2 mol L^{-1} , based on element S) as the electrolyte, and pure PP as the separator. As shown in Figure S9, the redox current of $\text{Ni}_x\text{B}/\text{Ni}_3(\text{BO}_3)_2$ (2.5 A g^{-1}) is much lower than $\text{C}/\text{Ni}_3\text{ZnC}_{0.7}\text{-B1}$ (7.9 A g^{-1}), indicating that the enhanced catalytic activity mainly comes from the Ni vacancies and optimized $\text{Ni}^{2+}/\text{Ni}(0)$ structures rather $\text{Ni}_x\text{B}/\text{Ni}_3(\text{BO}_3)_2$ phase.

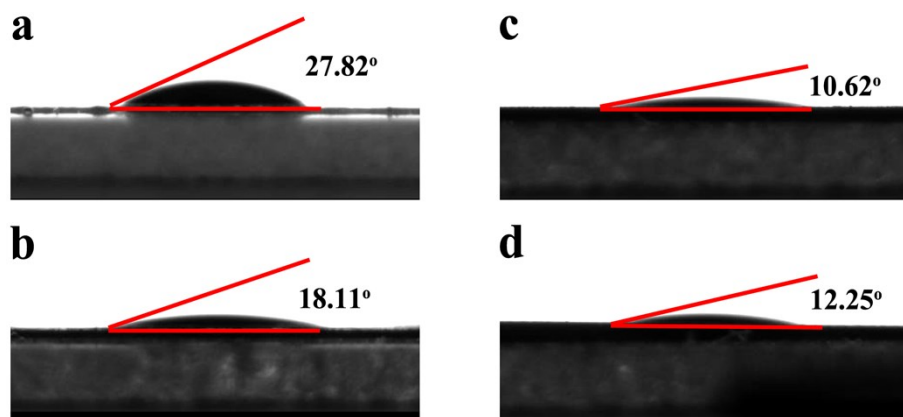


Figure S10. (a-d) The contact angles of pure PP, C/Ni₃ZnC_{0.7}@PP, C/Ni₃ZnC_{0.7}-P5@PP and C/Ni₃ZnC_{0.7}-B1@PP, respectively.

Table S3. EIS fitting results of pristine cells with C/Ni₃ZnC_{0.7}@PP, C/Ni₃ZnC_{0.7}-P5@PP and C/Ni₃ZnC_{0.7}@PP and pure PP separator.

Sample	R_s/Ω	R_{surf}/Ω	R_{ct}/Ω
Pure PP	2.01	19.45	15.86
C/Ni₃ZnC_{0.7}@PP	2.76	14.13	6.65
C/Ni₃ZnC_{0.7}-P5@PP	1.94	12.85	6.02
C/Ni₃ZnC_{0.7}-B1@PP	1.95	11.01	5.08

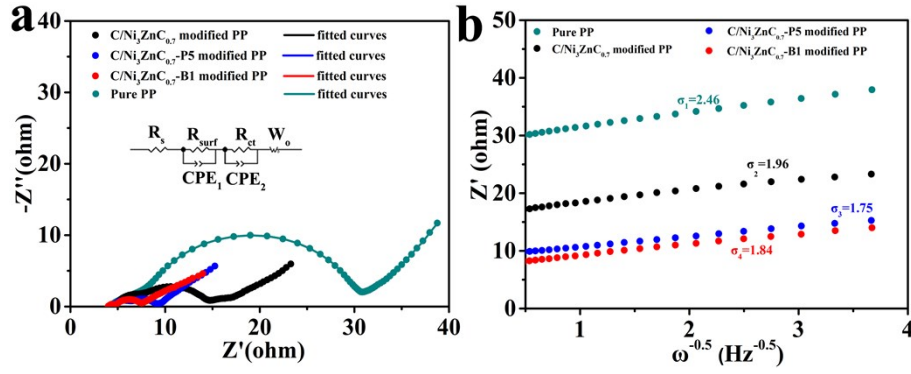


Figure S11. EIS fitting results of cells with C/Ni₃ZnC_{0.7}@PP, C/Ni₃ZnC_{0.7}-P5@PP and C/Ni₃ZnC_{0.7}-B1@PP and pure PP separator after cycling.

Table S4. EIS fitting results of cells with C/Ni₃ZnC_{0.7}@PP, C/Ni₃ZnC_{0.7}-P5@PP and C/Ni₃ZnC_{0.7}-B1@PP and pure PP separator after cycling.

Sample	R_s/Ω	R_{surf}/Ω	R_{ct}/Ω
Pure PP	4.26	4.14	21.66
C/Ni ₃ ZnC _{0.7} @PP	4.84	1.73	6.76
C/Ni ₃ ZnC _{0.7} -P5@PP	4.81	2.31	2.00
C/Ni ₃ ZnC _{0.7} -B1@PP	4.11	0.48	2.33

After cycling, the internal resistances R_s of all these cells increase (Figure S11 a-b and Table S3), but the cell with C/Ni₃ZnC_{0.7}-B1@PP exhibits smallest internal resistance R_s (4.11 Ω). Besides, the C/Ni₃ZnC_{0.7}-B1 modification layer contributes to the smaller Warburg coefficient ($\sigma_4=1.84$), demonstrating the fast solid-diffusion of Li ions going through the solid C/Ni₃ZnC_{0.7}-B1 modification layer. More importantly, the cell with C/Ni₃ZnC_{0.7}-B1 modification layer also exhibits much decreased charge transfer resistance R_{ct} (2.33 Ω). The fast-paced charge transfer behavior is conducive to boosting the conversion kinetics of polysulfides.

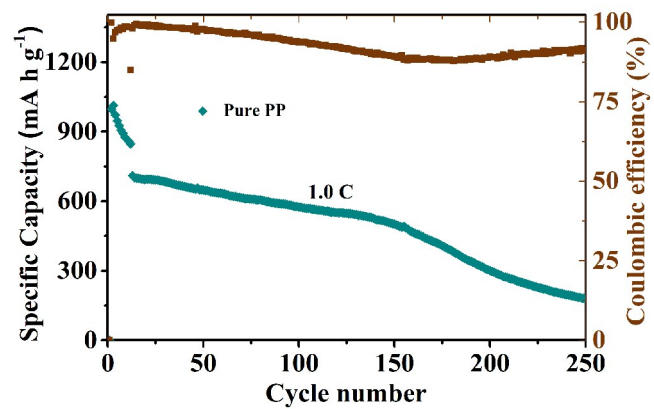


Figure S12. The cycling performance of the cell using pure PP separator.

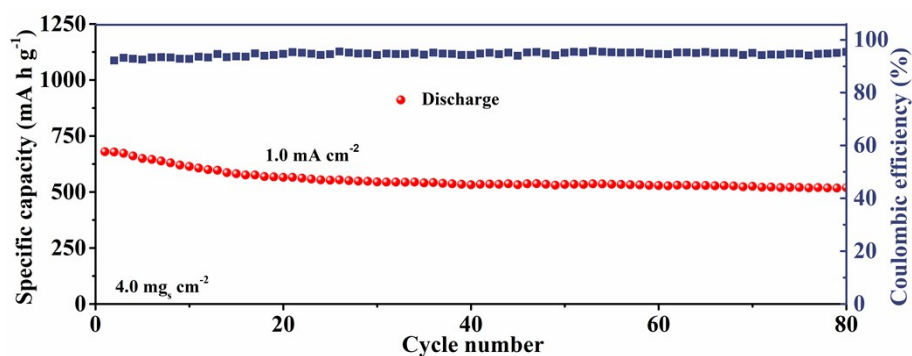


Figure S13. Cycling performance of the cell using C/Ni₃ZnC_{0.7}-B1 modified PP separator at 1.0 mA cm⁻² with a sulfur loading of 4.0 mg cm⁻².

Reference

- 1 W. J. Jiang, S. Niu, T. Tang, Q. H. Zhang, X. Z. Liu, Y. Zhang, Y. Y. Chen, J. H. Li, L. Gu, L. J. Wan and J. S. Hu, *Angew. Chem. Int. Ed.*, 2017, **56**, 6572-6577.
- 2 O. Akdim, R. Chamoun, U. B. Demirci, Y. Zaatar, A. Khoury and P. Miele, *Int. J. Hydrogen Energy*, 2011, **36**, 14527-14533.
- 3 H. Song, J. Su and C. Wang, *ACS Appl. Energy Mater.*, 2018, **1**, 5008-5015.
- 4 P. Zhang, M. Wang, Y. Yang, T. Yao, H. Han and L. Sun, *Nano Energy*, 2016, **19**, 98-107.
- 5 X. Liang, C. Hart, Q. Pang, A. Garsuch, T. Weiss and L. F. Nazar, *Nat Commun*, 2015, **6**, 5682.
- 6 S. Wang, J. Liao, X. Yang, J. Liang, Q. Sun, J. Liang, F. Zhao, A. Koo, F. Kong, Y. Yao, X. Gao, M. Wu, S. Z. Yang, R. Li and X. Sun, *Nano Energy*, 2019, **57**, 230-240.
- 7 X. Chen, Z. Yu, L. Wei, Z. Zhou, S. Zhai, J. Chen, Y. Wang, Q. Huang, H. E. Karahan and X. Liao, *J. Mater. Chem. A*, 2019, **7**, 764-774.